Article

Fluorescence Light-up Biosensor for MicroRNA Based on the Distance-Dependent Photoinduced Electron Transfer

Shasha Lu, Shuang Wang, Jiahui Zhao, Jian Sun, and Xiurong Yang

Anal. Chem., **Just Accepted Manuscript** • DOI: 10.1021/acs.analchem.7b01900 • Publication Date (Web): 14 Jul 2017

Fluorescence Light-up Biosensor for MicroRNA Based on the Distance-Dependent Photoinduced Electron Transfer

Shasha Lu,[†, ‡] Shuang Wang,[†, ‡] Jiahui Zhao, [†, §] Jian Sun,[†] and Xiurong Yang[*, †]

[†]State Key Laboratory of Electroanalytical Chemistry, Changchun Institute of Applied Chemistry, Chinese Academy of Sciences, Changchun, Jilin 130022, China

[‡]University of Science and Technology of China, Hefei, Anhui 230026, China

[§]University of Chinese Academy of Sciences, Beijing 100049, China

ABSTRACT: It is demonstrated that miRNAs exhibit significant regulatory roles in a series of biological processes and associated with diverse human diseases. Herein, we report a convenient fluorescent biosensor for the quantitative determination of miR-21, a key miRNA related to the cardio-cerebrovascular diseases. Our proposal involves not only the rational design of single stranded DNA as the probe, successively including a C-rich sequence as the synthetic template of DNA/Ag nanoclusters (DNA/AgNCs), a complementary (Com) sequence to hybridize with the miR-21 and a G-rich sequence to form complex of G-quadruplex/hemin, but also the distance-dependent property of photoinduced electron transfer (PET) between the preformed DNA/AgNCs (electron donor) and G-quadruplex/hemin complex (electron acceptor). In the presence of the target miR-21, the initial flexible single strand Com in the probe turns to the rigid Com/RNA heteroduplexes, and then the PET could be interrupted owing to the extended distance between the electron donor and acceptor, accompanying with the fluorescence quenching and recovery of DNA/AgNCs. Therefore, a fluorescence light-up biosensor for miR-21 could be developed through the monitoring of the degree of fluorescence recovery of DNA/AgNCs. Preferential to other previous PET-based detection methods, we construct the biosensor by utilizing the distance dependent property for the first time, and only need to adjust the sequences of Com in different miRNAs assays.

MicroRNAs (miRNAs) are a class of endogenous, noncoding, short single-stranded RNA molecules with a length of 20-24 nucleotides. By specifically binding to the target messenger RNAs (mRNAs), they have exhibited significant regulatory roles in a series of biological processes, including the early development, cell proliferation, apoptosis, cell death, fat metabolism and cell differentiation.[1-3] In addition, many studies have shown that the aberrant expressions of miRNAs were associated with the diverse human diseases, such as cancers, malignancies, cardio-cerebrovascular diseases, and neurodegeneration. Indeed, several miRNAs could serve as the significant therapeutic biomarkers or even therapeutic targets in the early diagnosis and treatment of diseases. For example, the contents of specific miRNAs (miR-21, miR-499, miR-133a, miR-208a, miR-208b, and miR-1) have been confirmed to play critical roles in the early diagnosis and treatment of cardio-cerebrovascular diseases, especially acute myocardial infarction (AMI).[4-6] In this regard, the miR-21 is significantly down-regulated in infarcted areas, while such infarction might be inhibited by the overexpression of miR-21 with the help of the gene transfer of adenovirus-mediated miR-21.[4] On this account, several traditional miRNAs detection methods based on the real-time polymerase chain reaction, northern blotting, microarrays, bioluminescence, electrochemiluminescence and electrochemistry had been already developed in recent years.[7-10] Except for these traditional miRNAs detection methods, fluorescence technology was also considered to be a promising detection method.

As a convenient analytical tool for molecular recognition and biomedical diagnosis, fluorescence technology has been widely used in the detection of DNA or RNA owing to the inherent operational simplicity and high sensitivity. Most of current DNA/RNA fluorescent assays have referred to the regulation of nucleic acid secondary structures (especially G-quadruplex, i-motif, hairpin, stem-loop and so on), as well as the energy transfer process such as the fluorescence resonance energy transfer (FRET)[11, 12] and chemiluminescence resonance energy transfer (CRET)[13] between donor and acceptor. Meanwhile, inspired by its peroxidase-mimicking activities, the stable G-quadruplex/hemin complex had been already used as a catalytic label for the direct colorimetric or multiplexed CRET-based detection of DNA and other related targets.[14-16] Besides such peroxidase-mimicking activities, more interestingly, the G-quadruplex/hemin complex had the potential to act as the electron acceptor to quench efficiently the fluorescence of certain fluorophores, owing to the well-known electron accepting ability of the Fe(III)/Fe(II)-protoporphyrin IX center in the complex. Therefore, the G-quadruplex/hemin-based electron transfer (ET) has been presented and developed as a novel type of response mechanism in the fluorescence detection strategies. In 2010, Willner and co-workers demonstrated the ET process between CdSe/ZnS quantum dots (QDs) and G-quadruplex/hemin for the first time, and furthermore utilized such novel photophysical mechanism into the detection of target biomolecules.[17] In order to avoid the complex modification processes for establishing the relationship between QDs and G-quadruplex/hemin, another fluorescent materials, DNA-templated silver nanoclusters (DNA/AgNCs) have attracted great attention[18, 19] because of their simple synthesis, photostability, low toxicity, and especially the unity of

Scheme 1. (A) Schematic illustration of the analysis of miR-21 based on the distance-dependent PET between DNA/AgNCs and G-quadruplex/hemin. (B) Comparison of the energy levels of DNA/AgNCs and G-quadruplex/hemin corresponding to the PET process.

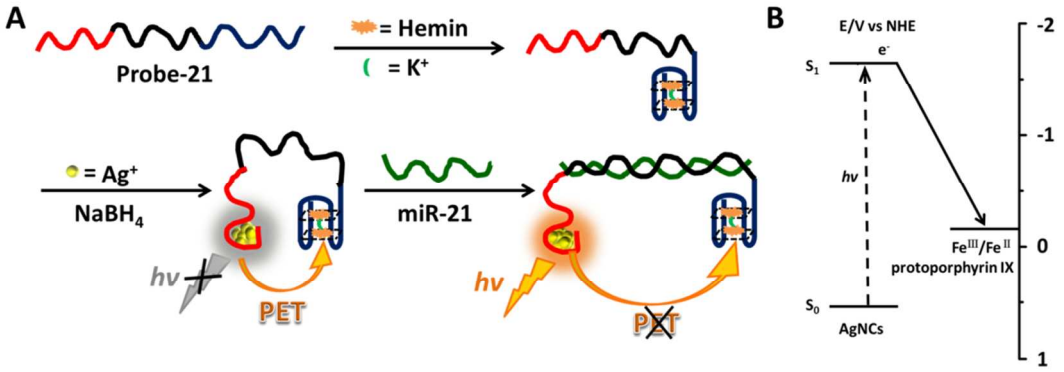

the donor and acceptor template (DNA sequences). Inspired by this, Wang et al. reported the proof-of-concept of photoinduced electron transfer (PET) between DNA/AgNCs and G-quadruplex/hemin, and used this novel G-quadruplex/hemin-based PET system to develop a molecular beacon for the detection of DNA and adenosine triphosphate.[20] However, both of the aforementioned detection strategies, along with several similar DNA-related bioassays,[21-23] mainly took advantage of the formation and dissociation of G-quadruplex/hemin, which was not preferred in practice due to the complexity of the sequence design in fact. Particularly noteworthy is that the PET process is directly related to the distance between DNA/AgNCs and G-quadruplex/hemin, where the quenching efficiency of PET decreased proportionally with increasing distance.[20] However, it is relatively scarce for applying the distance-dependent property of PET between DNA/AgNCs and G-quadruplex/hemin to establish a fluorescence biosensor for target biomolecules, especially DNA or RNA.

Inspired by the aforementioned G-quadruplex/hemin-based PET and its distance-dependent property, we present a novel conceptual fluorescent bioassay for the detection of miRNAs (miR-21 as a model) based on the distance adjustment of DNA/AgNCs and G-quadruplex/hemin herein. As shown in Scheme 1, we have designed and constructed a three segment nuclear acid probe (named as Probe-21), including a C-rich sequence (C, red part) as the synthetic template of DNA/AgNCs, a complementary sequence (Com, black part) to hybridize with the target miR-21 and a G-rich sequence (G, blue part) to form complex of G-quadruplex/hemin. Firstly, the addition of potassium ion (K^+) and hemin induces the formation of G-quadruplex/hemin complex, and then the fluorescent DNA/AgNCs can be synthetized by successively introducing $AgNO_3$ and $NaBH_4$ into the mixture solution. Under this circumstance, the Com section existed in the form of flexible single stranded, inducing a short distance between the electron donor (DNA/AgNCs) and receptor (G-quadruplex/hemin) of PET process as well as the relatively high fluorescence quenching efficiency. Upon the addition of target miR-21, the formation of the rigid DNA-RNA heteroduplexes could prop the Com section up, followed by the increment of the distance between the DNA/AgNCs and G-quadruplex/hemin. Furthermore, the increased distance would hinder the PET process, accompanied by the recovery of PET-quenched fluorescence of DNA/AgNCs. Meanwhile, the degree of fluorescence recovery of DNA/AgNCs is proportional to the increased concentration of the miR-21. As a result, the distance-dependent property of G-quadruplex/hemin-related PET has been applied to construct fluorescent biosensor for the first time, and a facile, simple and specific detection of miR-21 is readily achieved by monitoring the fluorescence intensity of DNA/AgNCs. Furthermore, our fluorescence light-up biosensor possesses the universal applicability for the detection of different miRNAs by only adjusting the sequences of Com section in the probes.

EXPERIMENTAL SECTION

Materials. All synthetic DNA/RNA and the miRNA extraction kit were ordered from Sangon Biotechnology Co. Ltd. (Shanghai, China). All of the DNA/RNA sequences used in this work were listed in Table S1. Hemin, silver nitrate ($AgNO_3$), sodium borohydride ($NaBH_4$) and diethy pyrocarbonate (DEPC) were obtained from Sigma-Aldrich (St. Louis, USA). All of other chemicals were of reagent grade and were used directly. The RNase free environment was created by DEPC solution (0.1% v/v). The ultrapure water (18.25 MΩ.cm, Millipore, USA) was used throughout all the experiments.

Instruments. Fluorescence measurements were carried out using an F-4600 fluorescence spectrophotometer (Hitachi) and the circular dichroism spectral measurements were performed on a Jasco J-820 Circular Dichroism Spectra polarimeter (Tokyo, Japan). FLS-920 Combined Steady State and Lifetime Spectrometer (Edinburgh, England) was used to measure time-resolved fluorescence. The atomic force microscopy (AFM) image was obtained by the Dimension Icon SPM (Bruker, Germany) at tapping mode in air. Transmission electron microscopy (TEM) measurements spectroscopy was taken on a Hitachi H-8100 EM with an accelerating voltage of 200 kV. The fluorescence quantum yield was performed on the FLS-980 Combined Steady State and Lifetime Spectrometer (Edinburgh, England). Cyclic voltammetric experiments were performed with a CHI 832C electrochemical analyzer (Chenhua Co., China). A three-electrode cell was used, which was consisted of a reference electrode (Ag/AgCl, saturated KCl), a counter electrode (platinum wire) and a working electrode (glassy carbon). The cell was deoxygenated with dry purified nitrogen (99.99%) before use and finishes the experiment in nitrogen atmosphere.

Synthesis of DNA/AgNCs.[20] A solution of $AgNO_3$ was added into the Probe-21, which was used as synthetic scaffold in phosphate buffer solution (20 mM, pH=7.4). One hour later,

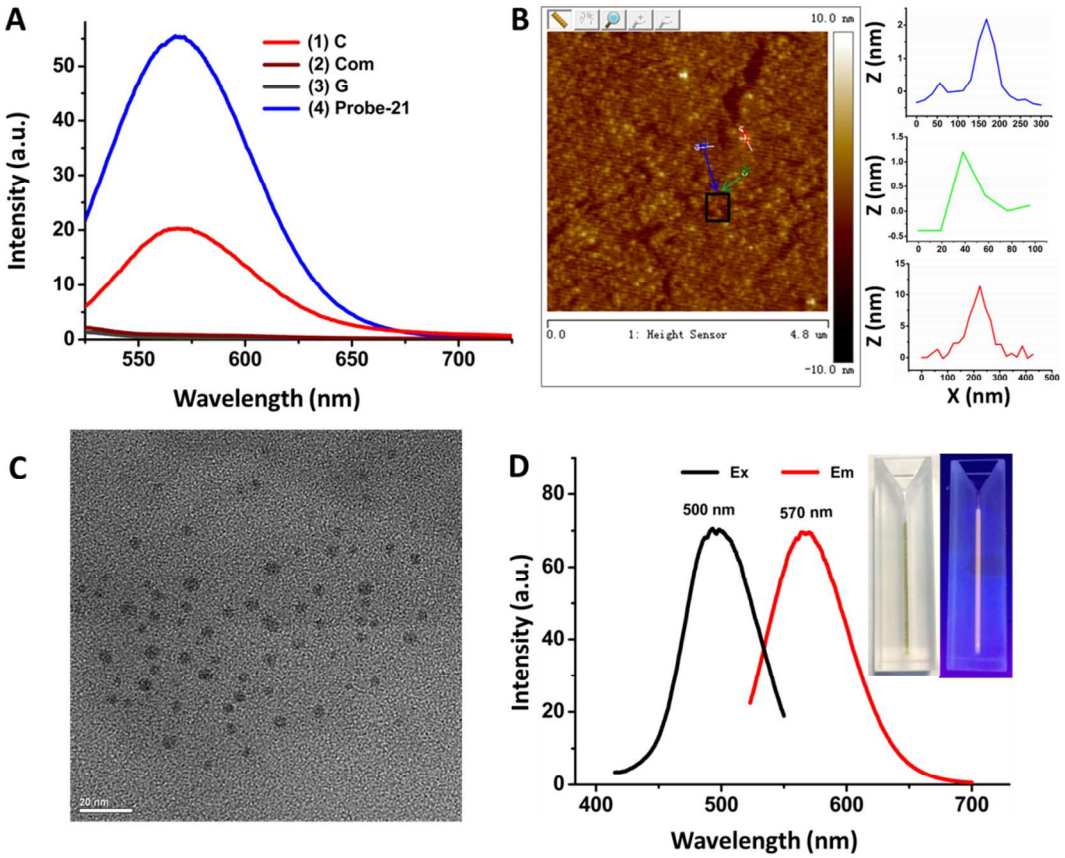

Figure 1. (A) Fluorescence emission spectra of DNA/AgNCs obtained using some fragments of Probe-21 (C, Com and G, repectively) and Probe-21 as the synthetic scaffold. (B) The AFM image of DNA/AgNCs and its cross-section analysis of different positions: AgNCs (blue curve), single DNA strands (green curve), and a small quantity of AgNPs (red curve). The black frame circled the DNA/AgNCs. (C) The TEM image of DNA/AgNCs. (D) Excitation and emission spectra of DNA/AgNCs obtained using Probe-21 as the synthetic scaffold. The inset showed the photographs of DNA/AgNCs under room light and UV irradiation.

the freshly prepared NaBH4 solution was added into the mixture and incubated in the dark at room temperature for another six hours to form DNA/AgNCs. The final concentration of Probe-21, $AgNO_3$ and $NaBH_4$ were 10 μM, 60 μM and 60 μM, respectively.

Fluorescent miR-21 Assays. In a typical miR-21 assay, the solutions of hemin and K^+ were firstly added to the Probe-21 in phosphate buffer solution (20 mM, pH=7.4). After being incubated at room temperature for two hours, a solution of $AgNO_3$ was added into the mixture. One hour later, freshly prepared $NaBH_4$ solution was introduced and incubated in the dark at room temperature for another six hours. The final concentrations of Probe-21, hemin, K^+, $AgNO_3$ and $NaBH_4$ were 10 μM, 10 μM, 0.5 M, 60 μM and 60 μM, respectively. Finally, different concentrations of miR-21 were added to the above solutions. After two hours incubation in the dark at room temperature, the fluorescence intensity was measured. In the experiment of feasibility, selectivity and specificity, the concentrations of DNA and miRNAs were both 10 μM.

MiRNAs Detection in Real Sample. MiRNAs extracted from human cervical cancer cells (Hela) and human breast adenocarcinoma cells (MCF-7) were selected as the real sample. After the cell counting process, miRNAs was extracted from different amounts of cells by the commercial miRNA extraction kit (Trizol Method). As a result, the miRNAs extracted from cells were dissolved in RNase-free water and the extraction solutions were used for miR-21 detection with the Probe-21.

RESULTS AND DISCUSSION

The Formation of fluorescent DNA/AgNCs. Due to the high affinity between Ag^+ and cytosine, the cytosine-rich single stranded DNA sequences were commonly used to synthesize fluorescent DNA/AgNCs in previous literatures.[20, 24, 25] As shown in Figure 1A, the DNA/AgNCs exhibiting an obvious fluorescence emission was successfully synthesized by employing a cytosine-rich single stranded DNA (5'-CCCCACCCCACCCCA-3', named C) as the template and $NaBH_4$ as the reducing agent, respectively. In contrast, no fluorescent product can be obtained if we choose the Com and G, which were used for miR-21 identification and G-quadruplex formation, instead of C under the similar conditions. Furthermore, our proposed Probe-21 (including section C, Com and G) was used as the template to prepare DNA/AgNCs and the resultant solution exhibited similar fluorescence peak to, but stronger intensity than that of C, which was attributed to the fact that G (the guanine-rich sequence) could greatly enhance the fluorescence of DNA/AgNCs synthesized by a cytosine-rich DNA.[26] In order to further study the properties of DNA/AgNCs synthesized by Probe-21, atomic force microscope (AFM) was used to characterize the DNA/AgNCs (Figure 1B). It could be seen that the DNA/AgNCs were dispersed with an average diameter of ~2

nm, which was consistent with the definition of nanoclusters (< 2 nm).[27] Furthermore, we could see a large number of DNA/AgNCs (black frame circled) were distributed evenly, which was a powerful proof that we have succeeded in synthesizing DNA/AgNCs, although there are a very little number of larger silver nanoparticles (AgNPs) or aggregates of AgNCs (red position). The TEM image of DNA/AgNCs in Figure 1C showed that the DNA/AgNCs with an average diameter of ~2 nm were uniform distribution, which was consistent with the AFM image. What's more, the excitation and emission spectra was shown in Figure 1D, the maximum emission of the DNA/AgNCs was shown at 570 nm when excited at 500 nm. The inset of Figure 1D showed the photographs of DNA/AgNCs under room light and UV irradiation, the bright orange under UV irradiation further confirmed the formation of fluorescent DNA/AgNCs. The fluorescence quantum yield (QY) of our DNA/AgNCs was measured to be 9.41%, which was a little lower compared to that of other DNA-templates AgNCs.[28-30] However, it looks like such value is enough to use the AgNCs as a fluorescent sensor in the following detection experiments.

The PET Process between DNA/AgNCs and G-quadruplex/hemin. The guanine-rich single stranded DNA sequences could fold to G-quadruplex structure in the present of K^+, following by the formation of the complex of G-quadruplex/hemin with the insert of hemin.[20-23] As we could see in Figure 2A, only in the presence of both K^+ and hemin, the fluorescence of DNA/AgNCs could be quenched by the preformed G-quadruplex/hemin complex (curve 3 vs. curve 1). It is suggested that the fluorescence quenching was induced by the formation of the G-quadruplex/hemin complex, which may related to the shortened distance between the hemin and the DNA/AgNCs.[20] In fact, we have also studied the effect of the order of formation of G-quadruplex/hemin complex and DNA/AgNCs on experimental results (Figure S1). In order to quantify the degree of fluorescence recovery after the addition of miR-21, we defined F_I as the initial fluorescence intensities of DNA/AgNCs in the absence K^+ and hemin. What's more, the F_0 and F were defined as fluorescence intensities of DNA/AgNCs before and after the addition of miR-21, respectively in the presence of G-quadruplex/hemin, the $(F-F_0)/F_0$ as the fluorescence recovery efficiency. On the basis of these definitions, we calculated the fluorescence recovery efficiencies of these systems and compared them with the fluorescence recovery efficiencies of Probe-21. Figure S1D showed the fluorescence recovery efficiencies of these systems. The order of G-quadruplex/hemin complex first obtained the maximum $(F-F_0)/F_0$ compared with the other two orders, which proved that the order will affect the experimental or analytical results. We attributed the reasons to the fact that the formation of G-quadruplex structure will not affect the formation of DNA/AgNCs and even be conducive to the synthesis of the DNA/AgNCs.

And then, the secondary structure changes of Probe-21 during the biosensor construction process were studied to confirm the formation of the G-quadruplex/hemin complex and DNA/AgNCs. As shown in Figure 2B, upon the addition of K^+ and hemin, the Probe-21 possesses a negative peak at approximately 240 nm and a positive peak at approximately 265 nm (curve 2), which were consistent with the CD spectra of a typical parallel G-quadruplex structure as previous literature reported.[31, 32] When we added the $AgNO_3$ and $NaBH_4$ to the Probe-21, the original peak of Probe-21 nearly disappeared (curve 1 changed to curve 3), suggested that the formation of DNA/AgNCs will disrupt the secondary structure of the Probe-21. However, the formed G-quadruplex structure of Probe-21 will not be destroyed by the DNA/AgNCs, and can maintain the second structure (curve 4). These results indicated that we have constructed both the G-quadruplex/hemin complex and DNA/AgNCs in the Probe-21 for our biosensor successfully.

In order to further explore the mechanism of fluorescence quenching, we next exhibited the UV-vis absorption spectra of the DNA/AgNCs and the G-quadruplex/hemin complex in Figure S2A. The G-quadruplex/hemin complex without any absorption peak in the fluorescence region of DNA/AgNCs, which ruled out the possibility of FRET.[33] In addition, we measured the lifetimes of DNA/AgNCs in the absence and presence of K^+/hemin, and the fluorescence lifetime of the DNA/AgNCs decreased when the K^+/hemin were added (Figure 2C). Furthermore, we found that the fluorescence lifetime of the DNA/AgNCs decreased with the increasement of hemin concentration (Figure S2B), which might be due to the fact that the photoexcited electrons were transferred from DNA/AgNCs to the Fe (III)/Fe (II)-protoporphyrin IX center of hemin.[20, 34] In addition, we introduced the cyclic voltammogram of DNA/AgNCs and hemin to discuss the energy levels of DNA/AgNCs and the redox state of the hemin in phosphate buffer solution on the glassy carbon electrode (Figure S3). The oxidation potential of DNA/AgNCs was gauged to be 0.315 V vs. Ag/AgCl [0.537 V vs. normal hydrogen electrode (NHE)], which was consistent with the previously reports.[20, 35] Furthermore, the reduction potential of the hemin was -0.384 V vs. Ag/AgCl (-0.162 V vs. NHE), corresponding to the Fe (III)/Fe (II)-protoporphyrin IX couple. The comparison of redox state of hemin and the energy level of DNA/AgNCs was depicted in Scheme 1B, implying that the photoexcited electrons of DNA/AgNCs could be transferred to the hemin, which was agreed with the hypothesis of fluorescence lifetime studies.

What's more, the PET efficiency, $(F_I-F_0)/F_I$, was used to judge the extent of fluorescence quenching. The addition of hemin only obtains the 11.6% of PET efficiency (Figure S4A), which was significantly lower than the PET efficiency (70%) when the G-quadruplex was introduced (Figure S4B). These results were consistent with the "hole hopping mechanism".[36] We also used different fragment combinations such as C + Com + G, (C + Com) + G, and C + (Com + G), instead of intact Probe-21 for feasibility studies (the detailed sequences shown in Table S1). As we could see in Figure S5, the addition of miR-21 could hardly enhance the fluorescence intensities in these systems, where the obtained $(F-F_0)/F_0$ were very small compared with that of Probe-21. These results were consistent with the "electron tunneling theory" and "self-consistent field theory",[37] as well as proved the distance-dependent PET mechanism further.

Feasibility Study. After that, we carried out experiments to verify the feasibility of our biosensor. We added the same amount of miR-21 to the as-prepared biosensor and the fluorescence was remarkably enhanced (curve 4 vs. curve 3, Figure 2A), proving that the PET-quenched fluorescence could be recovered by the addition of miR-21, the target hybridized with the Com section. Many previous studies have shown that the single stranded DNA (ssDNA) has strong molecular flexibility while the double stranded DNA (dsDNA) exhibits about 50 times stronger rigidity than ssDNA.[38, 39] Meantime, it has

been demonstrated that double stranded RNA exhibits stronger rigidity than double stranded DNA in general and the heteroduplexes of DNA and RNA has an intermediate behavior, with slightly closer to RNA than to DNA.[40] Therefore, the addition of miR-21 and subsequent formation of rigid Com/RNA heteroduplexes could greatly increase the distance between DNA/AgNCs and G-quadruplex/hemin complex and restore the PET-quenched fluorescence. Interestingly, the fluorescence emission wavelength had a red shift from 570 nm (curve 3) to 575 nm (curve 4) once the miR-21 was added, we suggested that this may be related to the enhanced rigidity of the Probe-21.[41] It was worth noting that the G-rich sequence didn't affect the fluorescence quenching and recovering of DNA/AgNCs, which indicated that the aforementioned fluorescence enhancement performance of the G to DNA/AgNCs only accounted for the secondary status compared with PET. We believe that this behavior could improve our detection sensitivity to some extent. In addition, the addition of miR-21 induce the positive CD peak at 265 nm of G-quadruplex moving towards the long wavelength direction (curve 5, Figure 2B), which could be attributed to the formation of DNA-RNA heteroduplexes, whose CD peak was usually around 270 nm.[42] This provided strong evidence for the successful hybridization between Com and miR-21.

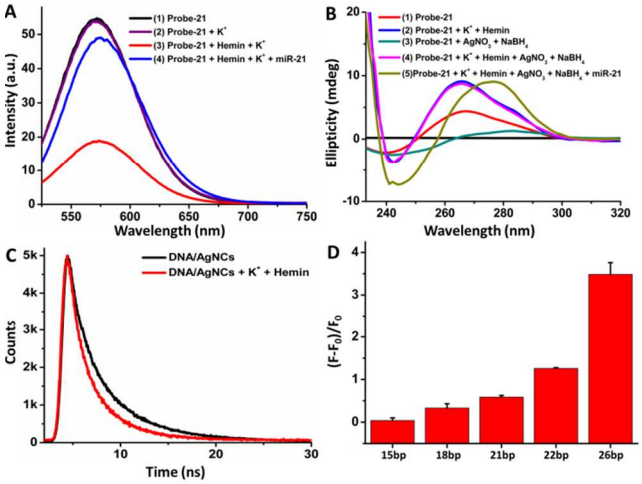

Figure 2. (A) Fluorescence emission spectra of DNA/Ag NCs obtained using Probe-21 as the synthetic scaffold under different circumstances. (B) CD spectra of DNA/AgNCs obtained using Probe-21 as the synthetic scaffold under different circumstances. (C) Fluorescence lifetimes of DNA/AgNCs in the absence (black line) and presence (red line) of K^+ and hemin. (D) The relationship of fluorescence recovery efficiency and length of the space between the DNA/AgNCs and the G-quadruplex/hemin.

It has been reported that the fluorescence efficiency of PET decreases with the increase of the distance between donor and acceptor. However, previous report only studied the case of less than or equal to 15 bp,[20] which was too short to apply to the detections of miRNAs (20-24 bp). In order to further explore the distance dependence property of PET process, we designed a series of bioprobes owning different lengths of Com (15-26 bp) corresponding to the target RNAs (15-26 bp), which could regulate the distance between the donor and acceptor of PET. The resultant fluorescence emission spectra and recovery efficiencies were shown in Figure S6 and Figure 2D respectively. All of these probes could synthesize fluorescent DNA/AgNCs (black curves, Figure S6) and the fluorescence could be quenched by G-quadruplex/hemin through PET process in the absence of corresponding target RNAs (red curves, Figure S6) regardless of the length of com. It is suggested that the length of ssDNA, with strong molecular flexibility, wouldn't influence the PET efficiency. However, the introduction of corresponding target RNAs would restore the fluorescence to the different degrees (blue curves, Figure S6). As we could see in Figure 2D, the $(F-F_0)/F_0$ was very close to zero when the distance was short (15 bp, ~ 5.2 nm for dsDNA) and enhanced with the increase of distance. When the distance increased to 22 bp (~ 7.5 nm), the fluorescence recovery efficiency could reach greater than 1, that was to say the increase of distance could inhibit the PET process in varying degrees, which further confirmed the distance-dependent PET mechanism as well as proved the feasibility of our biosensor for the miR-21 detection. What is more important, the platform could be applied to the detection of much longer RNA or even DNA by only adjusting the length and sequences of Com.

MiR-21 Detection Assay. In order to get the appropriate results, we optimized the experimental conditions before applying our platform in the detection of miR-21. Firstly, the effect of pH on the detection was investigated by using different pH phosphate buffer solution. As exhibited in Figure S7A, the fluorescence intensity of the resultant solutions decreased with the increase of pH, and that the fluorescence recovery efficiency increased with the increase of pH. Meanwhile, the fluorescence intensity was too weak when the pH ≥ 7.4, which was

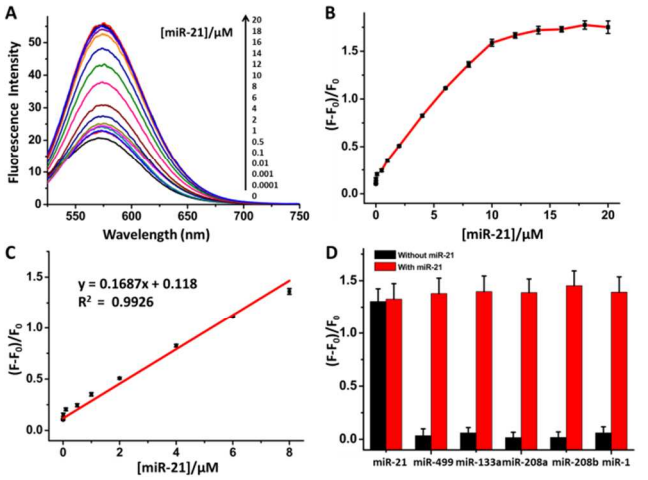

Figure 3. (A) Fluorescence emission spectra at different miR-21 concentrations (0, 0.0001, 0.001, 0.01, 0.1, 0.5, 1, 2, 4, 6, 8, 10, 12, 14, 16, 18 and 20 μM from bottom to top) obtained using Probe-21 as the synthetic scaffold in the presence of K^+ and hemin; (B) The relationship between the fluorescence recovery efficiency and the concentration of miR-21; (C) The linear relationship between the relative fluorescence intensity and the concentration of miR-21 over the concentration range from 0.1 nM to 8 μM. (D) The selectivity and interference studies of our biosensor.

not conducive to high sensitive detection. Therefore we chose the relatively neutral 7.4, whose fluorescence intensity and recovery efficiency were both relatively high. In addition, we also studied the relationship between the fluorescence intensity as well as the recovery efficiency and the concentration of hemin. As shown in Figure S7B, the fluorescence recovery efficiency first increased with the increase of hemin concentration, and decreased gradually after reaching the highest point.

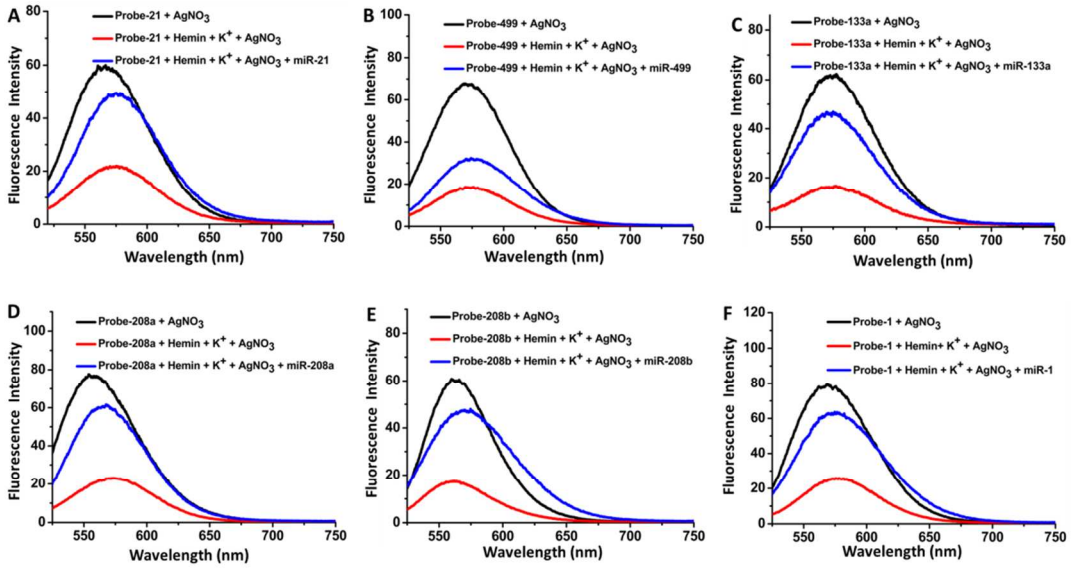

Figure 4. The fluorescence intensity when our system was used for the detection of miR-21 (A) and other acute myocardial infarction associated miRNA: (B) miR-499; (C) miR-133b; (D) miR-208a; (E) miR-208b; (F) miR-1.

The highest fluorescence recovery efficiency was at 10 μM (inset of Figure S7B), which was adopted in the following experiments.

Under the aformentioned optimized conditions, we applied the biosensor in the detection of miR-21. Different concentrations of miR-21 were added to the formed biosensor and the fluorescence emission spectra were shown in Figure 3A. As expected, the fluorescence intensity enhanced with the increasing concentration of miR-21 gradually, which indicated that the added miR-21 could hybridize with the Com and induce the recovery of the fluorescence quenched by the PET process. The fluorescence recovery efficiency enhanced along with the increased concentration of miR-21 when the concentration was less than 10 μM (Figure 3B). But it would not continue to increase with the increasement of concentration, which was consistent with the one to one hybridization relationship between miR-21 and Com. As shown in Figure 3C, a good linear range from 0.1 nM to 8 μM was obtained, and the detection limit could reach to 0.06 nM based on 3S/N.

Furthermore, the specificity and selectivity were also vital factors to evaluate a detection platform. In order to test the specificity and selectivity of our platform, several potentially interfering AMI-associated miRNAs such as miR-499, miR-133a, miR-208a, miR-208b, and miR-1 were also investigated and the results were shown in Figure 3D. Obviously, the biosensor could show higher fluorescence recovery efficiency only in the presence of miR-21, and other miRNAs wouldn't significantly affect the fluorescence recovery efficiency of miR-21. These results demonstrated that the biosensor exhibited excellent specificity and selectivity for the miR-21 detection.

Universality Study of Our Platform. Just as we mentioned above, the platform could be applied to the detection of other RNA or even DNA by only adjusting the length and sequences of Com. To validate the universal applicability, we designed a series of probes for other AMI-associated miRNAs (miR-499, miR-133a, miR-208a, miR-208b, and miR-1) just by integrating the corresponding complementary sequence in the nuclear acid probes instead of that of miR-21. As shown in Figure 4, the addition of corresponding miRNAs could restore the PET-quenched fluorescence of all probes. Furthermore, all of these miRNAs (21/22 bp) showed relative high fluorescence recovery efficiencies except miR-499 (21 bp) (Figure S8), which was partly consistent with the aformentioned result that fluorescence recovery efficiencies enhanced with the increase of distance. These results suggested that our detection assay was versatile and could be used to detect most of the miRNAs or longer DNA/RNA with high sensitivity only by adjusting the length and sequence of the Com.

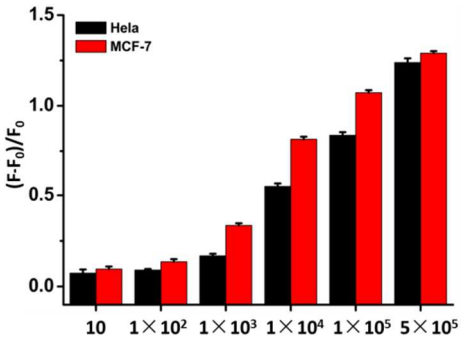

Figure 5. The application of our biosensor in the detection of miR-21 in human Hela and MCF-7 cell lines with 10, 1×10^2, 1×10^3, 1×10^4, 1×10^5, 5×10^5 cells, respectively.

MiR-21 Detection in Tumor Cells. In order to evaluate the feasibility of our biosensor in real samples, human cervical cancer cell line (HeLa) and human breast adenocarcinoma cells (MCF-7) were selected to measure the expression of miR-21. MiR-21 extracted from different numbers of cells was added to the as-prepared biosensor. As shown in Figure 5, the fluorescence recovery efficiencies increased with the increment of HeLa or MCF-7 cells number, which agreed with the fact that the amount of miR-21 was increased with the number of cells. Meanwhile, the fluorescence recovery efficiencies of HeLa cells were lower than the same numbers of the MCF-7 cells, which was consistent with the fact that the content of miR-21 in HeLa cells were indeed less than the same numbers

of the MCF-7 cells confirmed in previous reports.[43, 44] These results demonstrated the potential of our proposed system for the quantitative determination of miRNAs in tumor cells, which had very important significance for the early diagnosis of diseases.

CONCLUSIONS

In summary, we have proposed an original and exquisite miRNAs detection platform inspired by the distance-dependent property of PET between G-quadruplex/hemin complex and DNA/AgNCs for the first time. We firstly constructed a three-section single stranded DNA (C + Com + G) as the biosensor, and then prepared the G-quadruplex/hemin complex and DNA/AgNCs by G and C section, which were used as electron acceptors and donors for the following PET process respectively. The target miRNAs (miR-21 as a model) would hybridize with the flexible Com section, inhibiting the PET process and corresponding fluorescence quenching by the formation of rigid Com/RNA heteroduplexes. Based on the fact that miR-21 could specifically recover the fluorescence and the recovery efficiency increased with the increase of miR-21 concentration, the proposed three-section DNA-based bioprobe could be utilized in the quantitative determination of miR-21. Significantly, only by adjusting the sequence and length of Com, different miRNAs could be detected sensitively by using our developed platform. Furthermore, we also envision that our system holds great potential for the early clinical diagnostics of miRNAs-related diseases and opens an opportunity for the design of biosensors based on the distance-dependent property of PET.

ASSOCIATED CONTENT

Supporting Information

The Supporting Information is available free of charge on the ACS Publications website.

The fluorescence spectrum of different order in the formation process of PET system. UV−vis spectra of DNA/AgNCs and G-quadruplex/hemin complex, the lifetimes of DNA/AgNCs in the presence of various concentrations of hemin, cyclic voltammogram of DNA/AgNCs and hemin, optimization of pH and hemin concentration, various control experiments and all DNA/RNA sequences (Microsoft Word 2010).

AUTHOR INFORMATION

Corresponding Author

*Prof. Xiurong Yang, State Key Laboratory of Electroanalytical Chemistry, Changchun Institute of Applied Chemistry, Chinese Academy of Sciences. E-mail: xryang@ciac.ac.cn. Tel.: +86 431 85262056; Fax: +86 431 85689278.

Notes

The authors declare no competing financial interest.

ACKNOWLEDGMENT

This work was supported by the National Key Research and Development Program of China (2016YFA0201301), the National Natural Science Foundation of China (Grant Nos. 21435005, 21627808, 21605139), and Key Research Program of Frontier Sciences, CAS (QYZDY-SSW-SLH019).

REFERENCES

(1) Zhang, P.; He, Z.; Wang, C.; Chen, J.; Zhao, J.; Zhu, X.; Li, C.-Z.; Min, Q.; Zhu, J.-J. *ACS Nano* **2015,** 9 (1), 789-798.

(2) Dong, H.; Meng, X.; Dai, W.; Cao, Y.; Lu, H.; Zhou, S.; Zhang, X. *Anal. Chem.* **2015,** 87 (8), 4334-4340.

(3) Shu, D.; Li, H.; Shu, Y.; Xiong, G.; Carson, W. E.; Haque, F.; Xu, R.; Guo, P. *ACS Nano* **2015,** 9 (10), 9731-9740.

(4) Dong, S.; Cheng, Y.; Yang, J.; Li, J.; Liu, X.; Wang, X.; Wang, D.; Krall, T. J.; Delphin, E. S.; Zhang, C. *J. Biol. Chem.* **2009,** 284 (43), 29514-29525.

(5) Liu, X.; Fan, Z. W.; Zhao, T. S.; Cao, W.; Zhang, L.; Li, H.; Xie, Q.; Tian, Y.; Wang, B. C. *Exp. Gerontol.* **2015,** 72, 230-238.

(6) Kuwabara, Y.; Ono, K.; Horie, T.; Nishi, H.; Nagao, K.; Kinoshita, M.; Watanabe, S.; Baba, O.; Kojima, Y.; Shizuta, S.; Imai, M.; Tamura, T.; Kita, T.; Kimura, T. Circ-Cardiovasc. *Gene.* **2011,** 4 (4), 446-U287.

(7) Zheng, W. D.; Di, Y. W.; Liu, Y. H.; Huang, G.; Zheng, Y. W.; Zhang, Y.; Fang, W. *Clin. Biochem.* **2013,** 46 (15), 1566-1571.

(8) Cissell, K. A.; Rahimi, Y.; Shrestha, S.; Hunt, E. A.; Deo, S. K. *Anal. Chem.* **2008,** 80 (7), 2319-2325.

(9) Chen, A.; Ma, S.; Zhuo, Y.; Chai, Y.; Yuan, R. *Anal. Chem.* **2016,** 88 (6), 3203-3210.

(10) Dong, H.; Jin, S.; Ju, H.; Hao, K.; Xu, L.-P.; Lu, H.; Zhang, X. *Anal. Chem.* **2012,** 84 (20), 8670-8674.

(11) Degliangeli, F.; Kshirsagar, P.; Brunetti, V.; Pompa, P. P.; Fiammengo, R. *J. Am. Chem. Soc.* **2014,** 136 (6), 2264-2267.

(12) Qiu, X.; Hildebrandt, N. *ACS Nano* **2015,** 9 (8), 8449-8457.

(13) Freeman, R.; Liu, X.; Willner, I. *J. Am. Chem. Soc.* **2011,** 133 (30), 11597-11604.

(14) Fu X., Gu D. Y., Zhao S. D., Wen S. T., Zhang H. *Chinese J. Anal. Chem.* **2016,** 44(10), 1487-1494.

(15) Li, T.; Dong, S.; Wang, E. *Anal. Chem.* **2009,** 81 (6), 2144-2149.

(16) Liu, X.; Freeman, R.; Golub, E.; Willner, I. *ACS Nano* **2011,** 5 (9), 7648-7655.

(17) Sharon, E.; Freeman, R.; Willner, I. *Anal. Chem.* **2010,** 82 (17), 7073-7077.

(18) Yeh, H.-C.; Sharma, J.; Shih, I.-M.; Vu, D. M.; Martinez, J. S.; Werner, J. H. *J. Am. Chem. Soc.* **2012,** 134 (28), 11550-11558.

(19) Shamsipur, M.; Molaabasi, F.; Hosseinkhani, S.; Rahmati, F. *Anal. Chem.* **2016,** 88 (4), 2188-2197.

(20) Zhang, L.; Zhu, J.; Guo, S.; Li, T.; Li, J.; Wang, E. *J. Am. Chem. Soc.* **2013,** 135 (7), 2403-2406.

(21) Zhang, K.; Wang, K.; Zhu, X.; Gao, Y.; Xie, M. *Chem. Commun.* **2014,** 50 (91), 14221-14224.

(22) Wang, G.; Zhu, Y.; Chen, L.; Zhang, X. *Biosens. Bioelectron.* **2015,** 63, 552-557.

(23) Wang, G.-L.; Shu, J.-X.; Dong, Y.-M.; Wu, X.-M.; Zhao, W.-W.; Xu, J.-J.; Chen, H.-Y. *Anal. Chem.* **2015,** 87 (5), 2892-2900.

(24) Zhang, L.; Liang, R.-P.; Xiao, S.-J.; Bai, J.-M.; Zheng, L.-L.; Zhan, L.; Zhao, X.-J.; Qiu, J.-D.; Huang, C.-Z. *Talanta* **2014,** 118, 339-347.

(25) Shah, P.; Choi, S. W.; Kim, H.-j.; Cho, S. K.; Bhang, Y.-J.; Ryu, M. Y.; Thulstrup, P. W.; Bjerrum, M. J.; Yang, S. W. *Nucleic Acids Res.* **2016,** 44 (6), e57.

(26) Zhang, J.; Li, C.; Zhi, X.; Ramón, G. A.; Liu, Y.; Zhang, C.; Pan, F.; Cui, D. *Anal. Chem.* **2016,** 88 (2), 1294-1302.

(27) Yang, X.; Gan, L.; Han, L.; Wang, E.; Wang, J. *Angew. Chem., Int. Ed.* **2013,** 52 (7), 2022-2026.

(28) Yuan, Z.; Chen, Y.-C.; Li, H.-W.; Chang, H.-T, *Chem. Commun.* **2014,** 50 (69), 9800-9815.

(29) Guo, W.; Yuan, J.; Dong, Q. Wang, E. *J. Am. Chem. Soc.* **2013,** 132 (3), 932-934.

(30) Zhang, L.; Wang, E. *Nano Today* **2014,** 9 (1), 132-157.

(31) Deng, M.; Zhang, D.; Zhou, Y.; Zhou, X. *J. Am. Chem. Soc.* **2008,** 130 (39), 13095-13102.

(32) Dash, J.; Waller, Z. A. E.; Pantos, G. D.; Balasubramanian, S. *Chem-Eur. J.* **2011,** 17 (16), 4571-4581.

(33) Clapp, A. R.; Medintz, I. L.; Mauro, J. M.; Fisher, B. R.; Bawendi, M. G.; Mattoussi, H. *J. Am. Chem. Soc.* **2004,** 126 (1), 301-310.

(34) Patel, S. A.; Cozzuol, M.; Hales, J. M.; Richards, C. I.; Sartin, M.; Hsiang, J. C.; Vosch, T.; Perry, J. W.; Dickson, R. M. *J. Phys. Chem. C* **2009,** 113 (47), 20264-20270.

(35) Sharma, J.; Rocha, R. C.; Phipps, M. L.; Yeh, H.-C.; Balatsky, K. A.; Vu, D. M.; Shreve, A. P.; Werner, J. H.; Martinez, J. S. *Nanoscale* **2012,** 4 (14), 4107-4110.
(36) Giese, B. *Curr. Opin. Chem. Biol.* **2002,** 6 (5), 612-618.
(37) Beratan, D. N.; Skourtis, S. S. *Curr. Opin. Chem. Biol.* **1998,** 2 (2), 235-243.
(38) Wang, C.; Yuan, X.; Liu, X.; Gao, Q.; Qi, H.; Zhang, C. *Anal. Chim. Acta* **2013,** 799, 36-43.
(39) Skinner, G. M.; van den Hout, M.; Broekmans, O.; Dekker, C.; Dekker, N. H. *Nano Lett.* **2009,** 9 (8), 2953-2960.
(40) Noy, A.; Perez, A.; Marquez, M.; Luque, F. J.; Orozco, M. *J. Am. Chem. Soc.* **2005,** 127 (13), 4910-4920.
(41) Liu, B.; Yu, W.-L.; Pei, J.; Liu, S.-Y.; Lai, Y.-H.; Huang, W. *Macromolecules* **2001,** 34 (23), 7932-7940.
(42) O'Neil, M. A.; Barton, J. K. *J. Am. Chem. Soc.* **2002,** 124 (44), 13053-13066.
(43) Yin, B.-C.; Liu, Y.-Q.; Ye, B.-C. *J. Am. Chem. Soc.* **2012,** 134 (11), 5064-5067.
(44) Liao, Y.; Huang, R.; Ma, Z.; Wu, Y.; Zhou, X.; Xing, D. *Anal. Chem.* **2014,** 86 (9), 4596-4604.

For TOC only